Journal of Applied Mechanics and Technical Physics, Vol. 48, No. 1, pp. 11–16, 2007

MODELING JET FLOWS CAUSED BY THE INCIDENCE OF A SHOCK WAVE ON A PROFILED FREE SURFACE

V. A. Ogorodnikov, A. L. Mikhailov, A. V. Romanov, A. A. Sadovoi, S. S. Sokolov, and O. A. Gorbenko

UDC 620.178.7

The problem of the incidence of a shock wave with a front-pressure amplitude of about 30 GPa *at the profiled free surface of an aluminum sample is studied. It is shown that in the case of large perturbations* (*amplitude* 1 mm *and wavelength* 10 mm)*, jet flows occur on the free surface. The data obtained are described using a kinetic fracture model that takes into account the damage initiation and growth in the material due to tensile stress and shear strain.*

Key words: *shock wave, free surface, perturbations, jet flows, tensile stress, shear strain.*

The normal incidence of a shock wave (SW) on the free surface (FS) of a condensed material sample without macroscopic features can lead to a number of effects due to the deviation of the SW velocity from the doubling law, velocity dispersion, particle ejection (dusting) from the FS [1–3]. However, the FS can have macroscopic features in the form of defects, artificial conical or hemispherical cavities and attached masses or a certain profile of, for example, a sinusoidal shape, whose amplitude a and wavelength λ far exceed the parameters characteristic of the FS microrelief. The occurrence of microroughness is due to the surface finish ($a \gg R_z$ and $\lambda \gg R_z$, where R_z is the height of the surface microroughness). The incidence of a SW on a FS with defects, cavities, and attached masses is accompanied by ejection of cumulative flows of particles [4–6], which complicates the numerical modeling and prediction of the fragmentation and dispersion of structural materials under shock-wave loading. The processes occurring on a profiled FS upon incidence of a SW, especially for $\lambda \gg a \gg R_z$, have been studied inadequately.

The present paper reports new experimental and calculation results from studies of the generation and propagation of perturbations caused by the incidence of a SW of intensity 30 GPa on the FS of AMts aluminum samples of sinusoidal shape with an initial amplitude $2a = 1$ mm and a wavelength $\lambda = 10$ mm. A diagram of the experiments is given in Fig. 1.

A cylindrical charge of a high explosive (HE) 120 mm in diameter and 60 mm high was initiated by a plane SW generator, which provided for a time difference for SW arrival at the sample of not more than 50 nsec. The FS of the sample in the form of a 130×130 mm plate 10 mm thick had cavities of sinusoidal shape, which allowed the use of a soft x-ray radiographic technique.

Figure 2 gives X-ray photographs obtained at various times in the experiments (the dashed curves are drawn over the convexities of the sample relief). An analysis of the X-ray photographs shows that the displacements of the FS of the sample by 5 and 12 mm relative to the initial position, which correspond to the times in the X-ray photographs $t_\gamma = 29$ and 31 μsec from the moment of HE initiation, leading jet flows are formed in the sample regions located under the initial concavities, and in the region of the initial convexities, there is deceleration of the sample material of lower density. The decreased density of the sample material observed in the X-ray photographs in the regions of convexities (Fig. 2b and c) is apparently caused by particle ejection (dusting) due to the microcumulation of particles resulting from the presence of the initial microrelief (in the experiments, the surface roughness was $R_z \leqslant 20$) [3]. Evidence for this is that in the regions located under the initial convexities, the velocity of the

Institute of Experimental Physics (VNIIEF), Sarov 607190; root@gdd.vniief.ru. Translated from Prikladnaya Mekhanika i Tekhnicheskaya Fizika, Vol. 48, No. 1, pp. 16–23, January–February, 2007. Original article submitted December 28; revision submitted March 10, 2006.

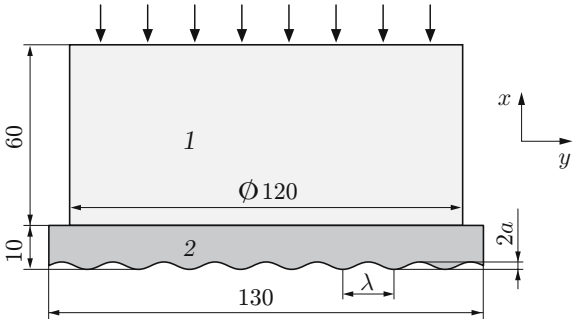

Fig. 1

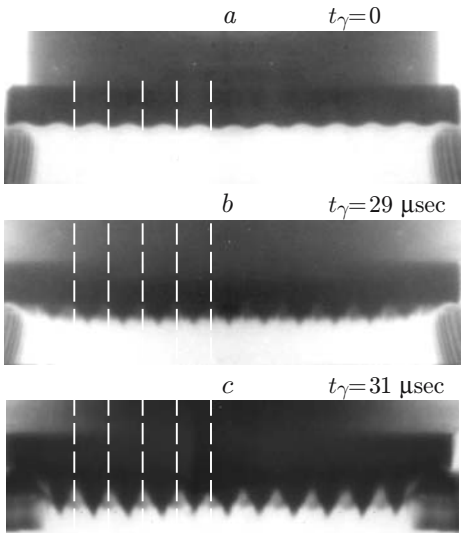

Fig. 2

Fig. 1. Diagram of experiments and calculations: 1) HE charge (50/50 TNT/RDX); 2) aluminum alloy sample; the arrows show the direction of the initiating SW.

Fig. 2. X-ray photographs of the free surface of the sample before loading (a) and for displacement of the free surface relative to the starting position by 5 (b) and 12 mm (c).

FS segments is 3.4 km/sec, i.e., it is somewhat higher than the calculated velocity of the continuous material of 3.2 km/sec under the given loading conditions. The change in the perturbation phase and the presence of jet flows in the regions located under the concave segments of the FS are caused by the effects of the velocity difference of the SW and the mass difference of the plate, which are described in detail in [7]. The velocity of these jet flows is 3.7 km/sec.

To test two-dimensional gas-dynamic problems and make a more detailed (compared to experiment) description of these problems, we carried out calculations using the DMK-UP technique for the conditions of the experiments performed [8]. This technique is employed for the numerical solution of two-dimensional problems of continuum mechanics, in particular, for the mathematical modeling of the generation and propagation of perturbations on irregular polygonal Lagrangian meshes. The calculations were performed taking into account the elastoplastic properties of the sample. Damage initiation and growth in the shock-loaded material were simulated using the kinetic fracture model of [9, 10], which describes fracture initiation and propagation in materials under tensile stresses and shear strain. The goal of these calculations was to estimate the range of applicability of the kinetic model for the description of fracture propagation in a shock-wave loaded sample with a specified initial profile and to determine the effect of the varied parameters on the generation and propagation of perturbations.

In the employed kinetic model, we introduce two parameters that characterize the rate of shear damage accumulation and the ultimate shear strain above which the sample begins to fail. The model uses the equation of state for the damaged material and takes into account the dependences of the dynamic yield stress and the dynamic viscosity on the damage. In addition, the dissipative losses due to the strength and viscosity of the damaged material and fracture on the adiabatic shear bands are successively taken into account. Fracture can occur by the viscoplastic growth of pores at tensile stresses (viscoplastic fracture) or by plastic shear strain (brittle fracture).

The computational scheme is presented in Fig. 1. The Chapman–Jouguet model with controlled detonation propagation velocity was used for detonation, the Zubarev equation of state [11] was used for the explosion products, and the properties of the alloy were described using the Mie–Grüneisen equation of state

$$p = p_{\text{cold}} + p_{\text{th}}.$$

Here p is the total pressure, p_{cold} and p_{th} are the cold and thermal pressures, respectively:

$$p_{\text{cold}} = \frac{\rho}{n}\, c_0^2 \Big[\Big(\frac{\rho}{\rho_0} \Big)^n - 1 \Big], \qquad p_{\text{th}} = \Gamma \rho (E - E_{\text{cold}}),$$

ρ and ρ_0 are the current and initial densities, c_0 is the sound velocity, n is a constant, $\Gamma = \gamma - 1$ is the Grüneisen coefficient, γ is the adiabatic exponent, and E is the energy. The following parameter values were used in the equation of state: $\rho_0 = 2.7$ g/cm^3, $c_0 = 5.5$ km/sec, $\gamma = 2.33$, and $n = 5.5$. For problems of this type, an important issues is a correct description of the SW profile. On an insufficiently detailed mesh, the SW front is smeared; therefore, for a correct description, a larger number of points is required.

The employed fracture model, as in [9], assumes that in the case of plastic fracture, defects (pores) have a spherical shape. Their size distribution is described by the formula

$$N(R) = N_0 \exp(-R/R_0),$$

where $N(R)$ is the number of defects with a size larger than R_0, N_0 is the total number of pores in unit volume, R_0 is the pore distribution parameter, and R is the pore size. The formation and growth of pores occur under the action of tensile stresses.

The differential equation describing the two stages of isotropic viscoplastic fracture, i.e., the initiation and growth of microdamage (microdamage growth occurs upon reaching the threshold negative pressure and the formation of new pores begins upon reaching a certain pressure value), can be written as

$$\frac{d\omega}{dt} = 8\pi \dot{N}_0 R_0^3 \exp\Big(- \frac{p_s - p_h}{p_1} \Big) H(p_s - p_h) + 3\omega\, \frac{p_s - p_{g0}}{4\eta}\, H(p_s - p_{g0}),$$

where ω is the degree of damage in the material under tensile stresses, $\dot{N}_0$ is the rate of pore formation, p_s is the pressure in the solid phase, p_h is the threshold pressure at which the formation of new pores begins, p_1 is the pressure determining the rate of pore formation under tensile stresses, p_{g0} is the negative threshold pressure at which microdamage growth is observed, $H(p_s - p_h)$ and $H(p_s - p_{g0})$ are unit Heaviside functions, and η is the viscosity of the material.

When the critical damage ω_0 is reached, the state of the material enters the stage of coalescence of microdefects and crack formation. The material ceases to resist expansion, i.e., fracture occurs. If the damaged medium begins to compress, irreversible bulk deformation of the fractured material occurs. The compaction-curve equation becomes

$$\omega(p) = \omega_0 (1 - p/p_{\text{c}})^2,$$

where ω_0 is the ultimate level of damage in the material below which compression strength begins to manifest itself in the fractured material and p_{c} is the compaction pressure. Compression can lead to full compaction to $\omega = 0$, and the further compression corresponds to the adiabatic curve of the continuous material.

The equation of state for the damaged medium, as in the NAG model [9], is written as

$$p(\rho, E, \omega) = (1 - \omega) p_s \Big(\frac{\rho}{1 - \omega}, E_s \Big),$$

where $p_s(\rho_s, E_s)$ is the equation of state for the continuous material, $\rho_s = \rho/(1 - \omega)$ is the density of the continuous material, and ρ is the average density of the medium in the cell.

The kinetic equation for the accumulation of the measure of damage α due to shear stress is written as

$$\dot{\alpha} = C \Big(\frac{S_u}{(1 - \omega)(1 - \alpha)} - S_u^* \Big) H \Big(\frac{S_u}{(1 - \omega)(1 - \alpha)} - S_u^* \Big),$$

where C and S_u^* are the model parameters for a particular material, $S_u = \sqrt{S_{ij} S_{ij}}$ is the intensity of the stress deviator, $S_{ij} = \sigma_{ij} - \sigma \delta_{ij}$ (σ is the average pressure, σ_{ij} is the stress tensor, and δ_{ij} is the Kronecker symbol), and $H(\alpha)$ is a unit Heaviside function.

In the given model, the variation in the properties of the medium during damage accumulation is described by the following relations:

$K = K_s(1 - \omega)$ for the bulk compression modulus;
$G = G_s(1 - \omega)(1 - \alpha)$ for the shear modulus;
$\eta = \eta_s(1 - \omega)(1 - \alpha)$ for the viscosity;
$Y = Y_s(1 - \omega)(1 - \alpha)$ for the yield stress.

TABLE 1

Number of Computation Points and Yield Stress of Aluminum

Calculation version	Number of points		Y_s, GPa
	Aluminum	HE	
1	248,228	82,203	0.26
2	248,228	186,277	0.26
3	248,228	20,782	0.50
4	248,228	20,782	0

TABLE 2

Parameters for Calculation of Isotropic Viscoplastic Fracture

Calculation version	p_1, GPa	η, Pa·sec
1	0.04	200
2	0.04	200
3	0.02	300
4	0.02	300

TABLE 3

Parameters for Calculation of Shear Fracture and Compaction

Calculation version	ρ_0, g/cm^3	c_n, km/sec	ε_0	p_c, GPa	G_s, GPa
1	2.7	10.4	0.05	10	27
2	2.7	10.4	0.05	—	27
3	2.7	20.4	0.05	—	27
4	2.7	20.4	0.05	—	27

Note. For all calculation versions, $\rho_0 = 2.7$ g/cm^3, $\omega_0 = 0.5$, $\dot{N}_0 = 0.3$ cm^3/sec, $R_0 = 10^{-4}$ cm, $p_{h0} = 0.3$ GPa, and $p_{g0} = 0.2$ GPa.

In the DMK technique, the measure of damage β due to shear strain is calculated as

$$\dot{\beta} = c_n(\varepsilon_p - \varepsilon_0)/[(1-\omega)(1-\beta-\alpha)].$$

Here c_n and ε_0 are model parameters for a particular material that characterize the fracture propagation rate and the ultimate strain corresponding to the onset of fracture in the cell; ε_p is the ultimate strain.

Shear fracture begins in the region of plastic strain upon reaching the ultimate strain. Fracture can also continue in the region of elastic strain. In this model, the variation in the properties of the medium during damage accumulation is described by the following relations:

$K = K_s(1-\omega)$ for the bulk compression modulus;
$G = G_s(1-\omega)(1-\beta-\alpha)$ for the shear modulus;
$\eta = \eta_s(1-\omega)(1-\beta-\alpha)$ for the viscosity;
$Y = Y_s(1-\omega)(1-\beta-\alpha)$ for the yield stress.

The calculations (version Nos. 1–4) were performed for four sets of parameters listed in Tables 1–3. In all calculations, it was assumed that the HE charge is initiated on its outer surface. In version 1, it is assumed that $p_c = 10$ GPa, and in version Nos. 2–4, compaction was ignored.

Figure 3 give calculation results (version No. 1) that correspond to the state of the sample near the profiled surface at various times. When the SW reaches the FS, an unloading wave forms and propagates into the sample. This leads to the occurrence of tensile stresses, resulting in the formation of fracture centers. On the profiled FS of the sample, unloading begins at different times, which causes the occurrence of shear strain. As a result, the fracture by both mechanisms is enhanced by virtue of the nonlinearity of the processes and local zones of fracture due to tensile and shear stresses are gradually developed in the sample. The data presented in Fig. 3 allow one to follow the dynamics of formation, growth, and coalescence of the damage zones due to the velocity difference of the shock-wave loading. The unloading wave profile at the time $t = 10$ μsec is shown in Fig. 3a. By that time, centers of tensile stress are formed in the sample (Fig. 3d), shear strain is absent (Fig. 3g), and the degree of damage is $\beta < 10^{-2}$. At later times $t = 11$ and 12 μsec, the complex interaction of the shock waves and unloading waves on the FS of the sample leads to the following effects: cumulative jets are formed near the initial concavities (Fig. 3b and c); a region of fracture due to tensile stress appears in the sample (Fig. 3e); shear strain is accumulated at the free surface near the initial concavities (Fig. 3h); the degree of damage due to shear strain reaches the ultimate value $\beta = 1$. By the time $t = 12$ μsec, the zones of fracture due to tensile stresses decrease considerably as a result of compaction and have a local nature (Fig. 3f, and the shear stresses reach the maximum value (Fig. 3i).

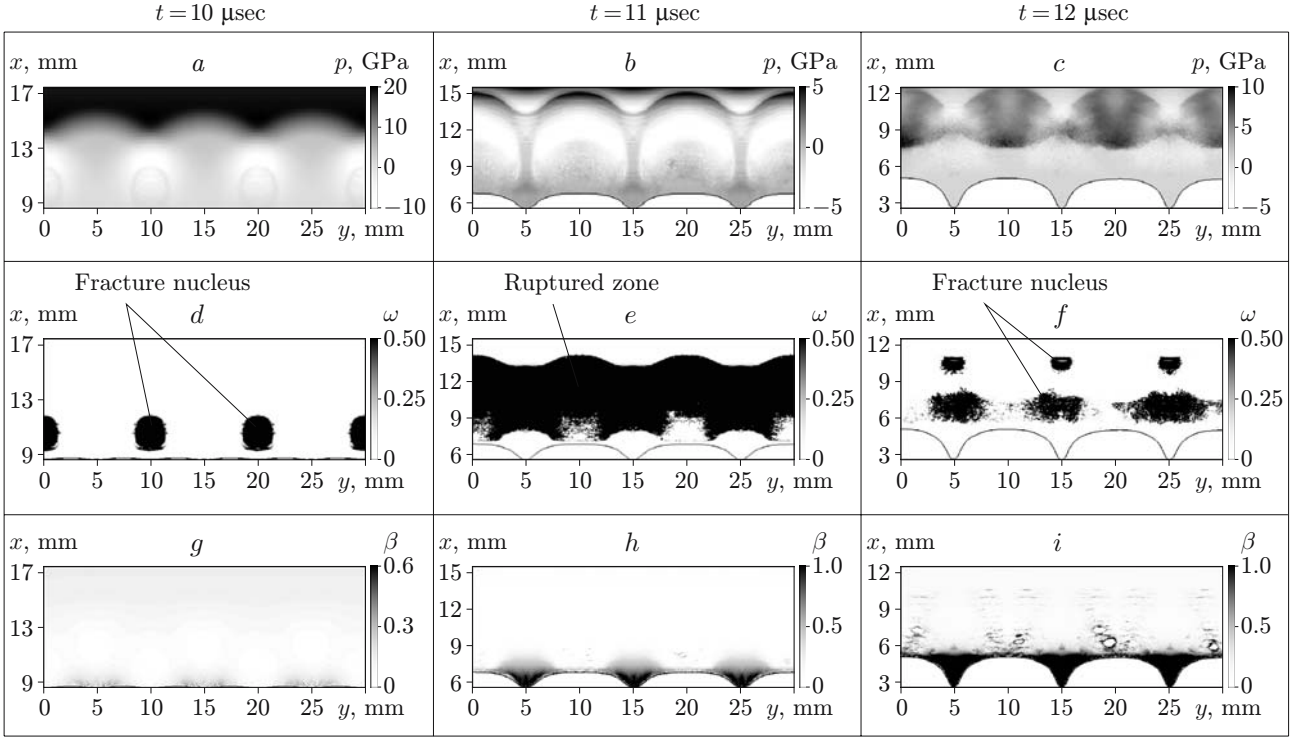

Fig. 3. State of the sample at various times (calculation): pressure distribution in a section of the sample (a–c), damage distribution due to tensile stress in the sample (d–f), and damage distribution due to shear strain in the sample (g–i).

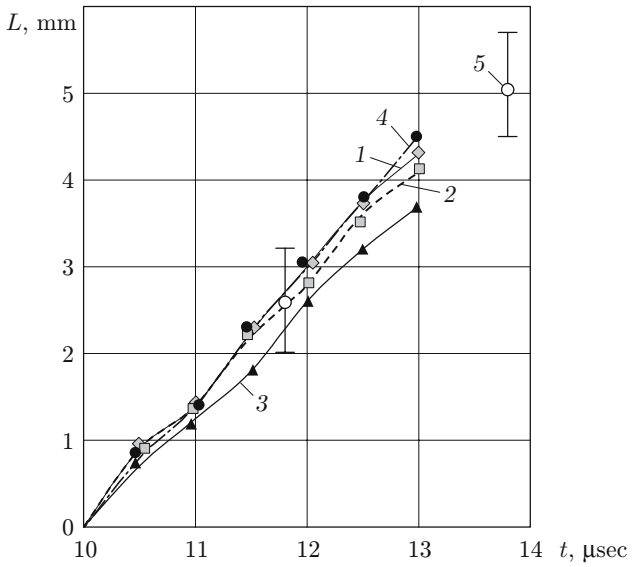

Fig. 4. Calculated time dependence of the jet length for various parameters of the fracture model: curves 1, 2, 3, and 4 refer to version Nos. 1, 2, 3, and 4, respectively in Tables 2 and 3; curve 5 refers to experimental data.

In the numerical modeling, the formation and development of local fracture centers depends on the chosen values of the model parameters. Figure 4 gives calculated dependences of the increment of the jet length L on time t near the initial concavity of the FS ignoring the compaction of the fractured material (version Nos. 2–4) and taking into account compaction for $p_c = 10$ GPa (version No. 1). Accounting for compaction increases the jet length by 5%. The influence of the yield stress on the calculated jet parameters was also studied. A twofold increase in the yield stress from 0.26 to 0.50 GPa (version No. 3) leads to a 15% decrease in the jet length. Calculation in the hydrodynamic approximation for $Y_s = 0$ (version No. 4) leads to a 20% increase in the jet length in comparison with version No. 3. In version Nos. 3 and 4, the rate of propagation of shear fracture was increased by approximately two times. In this case, the calculated jet parameters changed only slightly (by less than 1%).

An analysis of the numerical calculations performed shows that the compaction pressure and the yield stress of the material have the most substantial effect on the jet parameters. Much weaker influence on the calculated jet parameters is exerted by the shear fracture parameters, effective viscosity, and pressure, which determine the rate of pore formation in the presence of tensile stresses. We note that the main parameters of the kinetic fracture model were chosen from a large series of hydrodynamic experiments (see [3, 4, 9, 10], etc.).

Figure 4 also gives experimental data obtained by processing X-ray photographs (see Fig. 2). A comparison of the results of numerical calculations using the DMK technique and the experimental data shows that the kinetic fracture model [10] is adequate for describing perturbation propagation on the sinusoidal FS taking into account fracture due to tensile stresses near the initial convexities and shear strain near the initial concavities. The results suggest a possibility of a more detailed modeling of shock-induced fracture processes and fragmentation and dispersion of structural materials [12], especially in the near zone of explosions.

The modeling of the incidence of a SW on the sinusoidal FS for $a \gg R_z$ and $\lambda \gg R_z$ show that the qualitative picture of the process is the same as in the case of $a \approx R_z$ and $\lambda \approx R_z$, which is characterized by the presence of jet flows from the regions of the initial concavities.

REFERENCES

1. Ya. B. Zel'dovich and Yu. P. Raizer, *Physics of Shock Waves and High-Temperature Hydrodynamic Phenomena*, Academic Press, New York (1967).
2. A. K. Divanov, Yu. I. Meshcheryakov, and L. P. Fadeenko, "On the particle velocity distribution on the elastic precursor of a compression wave in aluminum," *Zh. Tekh. Fiz.*, **53**, No. 10, 2050–2054 (1983).
3. V. A. Ogorodnikov, A. G. Ivanov, A. L. Mikhailov, et al., "Particle ejection from the shocked free surface of metals and diagnostic methods for these particles," *Combust., Expl., Shock Waves*, **34**, No. 6, 696–700 (1998).
4. V. A. Ogorodnikov, A. G. Ivanov, and N. I. Kryukov, "Shock-wave dispersion of structural materials," *Combust., Expl., Shock Waves*, **35**, No. 5, 576–580 (1999).
5. A. G. Ivanov, L. I. Kochkin, V. A. Ogorodnikov, et al., "Characteristics of the acceleration of plates by a glancing detonation wave in the presence of an additional or concentrated mass," *Combust., Expl., Shock Waves*, **26**, No. 5, 612–614 (1990).
6. Yu. A. Trishin, *Physics of Cumulative Processes* [in Russian], Inst. of Hydrodynamics, Sib. Div., Russian Acad. of Sci., Novosibirsk (2005).
7. O. B. Drennov, A. L. Mikhailov, and V. A. Ogorodnikov, "Specification and evolution of local (periodic) perturbations in experimental studies of Rayleigh–Taylor instability in strong media," *J. Appl. Mech. Tech. Phys.*, **41**, No. 2, 362–366 (2000).
8. S. S. Sokolov, "Method for calculating two-dimensional nonstationary elastoplastic flows on irregular polygonal Lagrangian meshes," *Vopr. Atomn. Nauki Tekhn., Ser. Mat. Model. Fiz. Prots.*, No. 4, 62–80 (2004).
9. L. Seaman, D. R. Curran, and D. A. Shockey, "Computational models for ductile and brittle fracture," *J. Appl. Phys.*, **47**, No. 11, 4814–4826 (1976).
10. S. S. Sokolov, A. A. Sadovoi, and T. I. Chaika, "Mathematical modeling of the formation of high-velocity compact metal elements," *Vopr. Atomn. Nauki Tekhn., Ser. Mat. Model. Fiz. Prots.*, No. 3, 54–61 (2004).
11. M. V. Zhernokletov, V. N. Zubarev, and G. S. Telegin, "Expansion isentropes of the explosion products of condensed explosives," *J. Appl. Mech. Tech. Phys.*, No. 4, 650–655 (1969).
12. A. L. Mikhailov, V. A. Ogorodnikov, N. P. Khokhlov, et al., "Explosive fracture, fragmentation, and dispersion of structural materials," *Khim. Fiz.*, No. 8, 73–79 (2001).